Simulated performance of an ultracold ion source

Simulated performance of an ultracold ion source

S. B. van der Geer,[a] M. P. Reijnders, M. J. de Loos,[a] E. J. D. Vredenbregt, P. H. A. Mutsaers, and O. J. Luiten
Department of Applied Physics, Eindhoven University of Technology, P.O. Box 513, 5600 MB Eindhoven, The Netherlands

(Received 17 July 2007; accepted 13 September 2007; published online 7 November 2007)

At present, the smallest spot size which can be achieved with state-of-the-art focused ion beam (FIB) technology is mainly limited by the chromatic aberrations associated with the 4.5 eV energy spread of the liquid-metal ion source. Here we numerically investigate the performance of an ultracold ion source which has the potential for generating ion beams which combine high brightness with small energy spread. The source is based on creating very cold ion beams by near-threshold photoionization of a laser-cooled and trapped atomic gas. We present *ab initio* numerical calculations of the generation of ultracold beams in a realistic acceleration field and including all Coulomb interactions, i.e., both space charge effects and statistical Coulomb effects. These simulations demonstrate that with existing technology reduced brightness values exceeding 10^5 A m^{-2} sr^{-1} V^{-1} are feasible at an energy spread as low as 0.1 eV. The estimated spot size of the ultracold ion source in a FIB instrument ranges from 10 nm at a current of 100 pA to 0.8 nm at 1 pA. © *2007 American Institute of Physics*. [DOI: 10.1063/1.2804287]

I. INTRODUCTION

The nanometer milling capability of focused ion beam (FIB) technology has led to its widespread use in nanoscience in general and the semiconductor industry in particular.[1–4] The minimum focal spot size, and thus the minimum feature size which can be addressed, is ultimately limited by the quality of the ion source at a certain current. At present, the preferred source in a FIB is the liquid-metal ion source[1,5] (LMI) by virtue of its unrivalled beam brightness. For a gallium-based LMI the reduced brightness can be as high as 10^6 A m^{-2} sr^{-1} V^{-1} for a useable beam current of 10 pA and an energy spread of 4.5 eV.[1,5–7] A FIB equipped with a Ga-LMI enables a focal spot size of approximately 10 nm diameter, making it an indispensable tool for inspecting the smallest structures in present-day large-scale integrated circuits. However, if the advances in semiconductor technology keep up with Moore's law, 1-nm ion beam milling capability will be required within a few years time. The 10 nm spot size that can be achieved at present is mainly limited by chromatic aberrations associated with the 4.5 eV energy spread of the Ga-LMI.[8,9]

Recently, the ultracold ion source (UCI) was proposed as an alternative for the LMI.[10–12] The UCI has the potential of producing ion beams with a reduced brightness and useable current comparable to the LMI, but with a much smaller energy spread, and may therefore provide us with a route toward 1-nm ion beam milling. The UCI is based on creating very cold ion beams by near-threshold photoionization of a laser-cooled and trapped atomic gas.[13] So far several closely related schemes have been proposed. The original idea was to extract ions from a two-dimensionally laser-cooled atomic beam.[10] Subsequently, it was proposed to use a magneto-optical atom trap (MOT) as cold particle source, allowing both direct current and pulsed operation.[11] Very recently it was proposed to use a miniaturized MOT.[12] In Ref. 12 estimates were presented for the brightness, energy spread, and spot size that can be achieved, but without considering the effect of Coulomb interactions. In particular statistical Coulomb effects can severely degrade the quality of a charged particle beam. It is therefore worthwhile to assess the importance of such effects. Statistical Coulomb effects have been the subject of a great deal of theoretical study; see, for example, Ref. 14 for a recent review. Unfortunately, these theories are generally not suitable to predict source performance, since they cannot be applied to the critical initial acceleration stages.

Here we present a detailed particle tracking analysis of the UCI. The simulations start from conditions which can be realized routinely in a rubidium-based MOT.[13] Furthermore, realistic acceleration fields are used and all Coulomb effects are included, i.e., each and every individual ion is tracked from ionization to a field-free observation plane, while interacting with all other ions. This means that both long-range space-charge effects and statistical Coulomb effects, such as trajectory displacement and the Boersch effect,[14] are automatically accounted for in a fully exact manner. The results of the simulations are subsequently used to predict the performance of a Rb-based UCI in which ions are accelerated to 1 keV in a 100 kV/m extraction field, for beam currents ranging from 1 to 100 pA.

We find that for a useable beam current of 1 pA an energy spread as low as 0.1 eV is feasible, at reduced brightness values exceeding 10^5 A m^{-2} sr^{-1} V^{-1}, which is close to the fundamental thermal limit of a MOT-based ion source, as discussed in Ref. 12. Note that in Ref. 12 a definition for reduced (or normalized) brightness is used which differs by a factor $4\pi^2$ from the usual definition (see, e.g., Ref. 15, p.

[a]Also at: Pulsar Physics, Eindhoven, The Netherlands. http://www.pulsar.nl

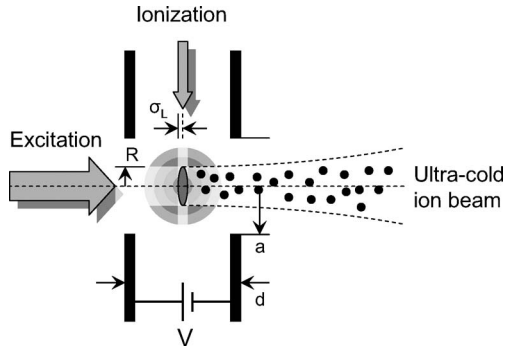

FIG. 1. Schematic of the laser-cooled ion source. The circular area represents a cloud of laser-cooled atoms. A small ionization volume is defined by first exciting the neutral atoms to an intermediate level, before they are ionized to just above threshold by a separate, perpendicular, ionization laser beam. The ions created are accelerated out of the ionization volume by the potential difference V.

976). For a proper comparison with our results their values of the reduced brightness should therefore be divided by a factor $4\pi^2$.

Our simulations also show that higher currents can be obtained at the cost of an increase in energy spread and a decrease in brightness. We find that the dependence of energy spread on current is very weak, in agreement with a simple model. The brightness decrease with current, however, is unexpected and dramatic: for a useable current of 100 pA the reduced brightness is more than an order of magnitude smaller than at 1 pA, in contradiction with a simple model,[12] in which the reduced brightness only depends on the initial atomic density and temperature in the MOT and not on current. We find that the decrease of the reduced brightness is due to disorder-induced heating of the transverse degrees of freedom,[16] which is the result of the initial random distribution of the ions.

II. SETUP

In a MOT the radiation pressure exerted by three orthogonal pairs of laser beams of pairwise opposite circular polarizations, in combination with a quadrupole magnetic field, cool the atoms to temperatures below 1 mK and cause the atoms to collect near the point in space where the magnetic field vanishes.[13] The resulting cloud of laser-cooled and trapped neutral atoms, suspended at the center of an accelerating structure, is schematically indicated by the concentric circles in Fig. 1.

The laser-cooled and trapped atoms are ionized in a two-step process,[17] as is shown in Fig. 1. In the first stage, the atoms are excited to an intermediate level by a laser beam that propagates along the symmetry axis of the accelerating structure. In the second step, atoms in the intermediate level are ionized by a second laser beam which is focused in one direction to a thin sheet beam, propagating at right angles with the first. The two-step ionization method allows control over both the shape and the dimensions of the initial ionization volume by carefully tuning the overlap of the excitation and ionization laser beams.

In the simulations in this paper the initial transverse density distribution of the ions is taken to be uniform with radius R. This can be accomplished by a uniform excitation laser profile with radius R, which is much smaller than the root-mean-squared (rms) size of the atom cloud. Atoms continuously enter the ionization volume from the sides due to thermal motion. Here we assume that the intensity of the ionization laser is adjusted such that the ionization time is comparable to the time it takes to cross the ionization volume. This results in a large fraction of the excited atoms getting ionized while the laser intensity is sufficiently low that the longitudinal density distribution can be assumed near-Gaussian with rms width σ_L as determined by the rms thickness of the ionizing sheet beam.

As is explained in Sec. III, it is advantageous to minimize the size of the ionization volume. For a current between 1 and 100 pA the typical size of the ionization volume ranges from a few to about a hundred micrometers across, much smaller than the typical dimensions of an atom cloud in a MOT. Ions can be extracted continuously from this small volume as long as the number of atoms extracted per unit time is less than the loading rate of the MOT in steady state. Even for currents as high as 1 nA this is not a limiting factor.

Immediately after creation, the ions are accelerated in an electrostatic field, created by a potential difference V across two metal electrodes surrounding the MOT, separated by a distance d, as is shown in Fig. 1. The laser-cooled ion-beam exits the source through a circular hole with radius a in the negative electrode.

III. FUNDAMENTAL PERFORMANCE LIMITS

A commonly used figure of merit for the transverse quality of nonrelativistic charged particle beams is the reduced brightness, B_r, defined in the conventional way as

$$B_r = \frac{1}{U}\frac{\partial^2 I}{\partial A\, \partial \Omega}, \tag{1}$$

where A is the cross-sectional area of the beam, Ω is the corresponding subtended solid angle, and U is the average kinetic energy. For an extended source emitting a uniform current density J at temperature T, the resulting brightness is given by[15]

$$B_r = \frac{Je}{\pi kT}, \tag{2}$$

where e is the elementary charge and k is the Boltzmann's constant. This equation shows that the maximum achievable beam brightness is fundamentally limited by the temperature and the available flux $\Phi = J/e$ of neutral atoms into the ionization volume.

In the case of a MOT the neutral atom flux is given by

$$\Phi_{\mathrm{MOT}} = 2\frac{n v_{\mathrm{th}}}{4}, \tag{3}$$

where n is the density of the trapped atoms and $v_{\mathrm{th}} = (8kT/\pi m)^{1/2}$ is the thermal velocity, with m as the atomic mass. The factor 2 in Eq. (3) originates from the fact that the influx can be from either side into the ionization volume. We thus find that for a MOT there is an upper bound to the brightness of the extracted beam that is independent of the

radius and that scales inversely proportional to the square root of the temperature

$$B_{r,\mathrm{MOT}} = \frac{2}{\pi}\frac{e^2 n}{\sqrt{2\pi mkT}}. \tag{4}$$

The initial rms energy spread σ_U is due to the combination of creating particles over a potential difference associated with the rms width σ_L of the ionizing sheet beam and the initial thermal motion of the ions with (atomic) temperature T. Let us first consider the case of zero initial temperature: If the initial ionization volume is located at the center of a diode with $a \ll d$, then the $T=0$ energy spread is given by

$$\sigma_{U_0} = eE_0\sigma_L, \tag{5}$$

where $E_0 \equiv V/d$. The corresponding $T=0$ rms longitudinal momentum spread is

$$\sigma_{p_0} = \frac{\sigma_{U_0}}{v_0} = \sqrt{\frac{meE_0\sigma_L^2}{d}}, \tag{6}$$

where $v_0 = \sqrt{eE_0 d/m}$ is the average velocity after acceleration. At finite initial temperature T, the thermal rms momentum spread $\sqrt{mkT}$ has to be added in quadrature to obtain the full rms longitudinal momentum spread

$$\sigma_p^2 = \sigma_{p_0}^2 + mkT. \tag{7}$$

However, for all cases of practical interest $mkT/\sigma_{p_0}^2 = dkT/eE_0\sigma_L^2 \ll 1$, so the thermal contribution can be neglected and the rms energy spread can be approximated by

$$\sigma_U \approx \sigma_{U_0} \equiv eE_0\sigma_L. \tag{8}$$

The width σ_L cannot be chosen arbitrarily small. The lowest energy spread occurs when the ionization sheet laser beam is focused such that its Rayleigh length is identical to the radius R of the excitation laser, leading to

$$\sigma_L \geq \sqrt{\lambda R/\pi}, \tag{9}$$

with λ as the wavelength of the ionization laser.

The maximum current that can be extracted from a uniformly emitting surface with radius R and flux Φ is given by $I = \Phi e \pi R^2$. According to Eqs. (8) and (9) the minimum energy spread for a given n and T increases with current, scaling with $I^{1/4}$ according to

$$\sigma_U \geq E_0\sqrt{\lambda R/\pi} = E_0\left(\frac{\lambda^2 I}{\pi^3 \Phi e}\right)^{1/4}. \tag{10}$$

A. Rubidium MOT as an ultracold ion source

In this paper we use initial conditions which are typical for a rubidium MOT, the workhorse of laser-cooling and trapping.[13] The excitation laser is tuned to the $^5P_{3/2}$ state of Rb, which implies that the ionization laser operates at $\lambda = 480$ nm. The limiting density in an atom trap is in the order of 10^{18} m^{-3} (Ref. 18) and a temperature $T = 200$ μK is routinely achieved in our laboratory. These values translate into a flux $\Phi = 10^{17}$ atoms m^{-2} s^{-1} and, hence, a brightness as high as 3×10^5 A m^{-2} sr^{-1} V^{-1}, see Eqs. (3) and (4). Combined with an electric field $E_0 = 100$ kV/m this results in an initial energy spread as low as 0.25 eV at currents as large as 100 pA, see Eq. (10).

Although these estimates of the initial low energy spread and high brightness of the UCI are very encouraging, it is not *a priori* clear that the earlier numbers can be realized in a realistic setup. Realistic acceleration fields and statistical Coulomb effects may decrease the brightness significantly.

IV. NUMERICAL APPROACH

The setup under investigation has been simulated with the GPT code.[19] This code solves the three-dimensional equations of motion of each and every ion, in terms of velocity $\mathbf{v}_i$ and position $\mathbf{r}_i$ of each particle $i = 1, 2, \cdots, N$, including all pairwise Coulomb interactions

$$m\ddot{\mathbf{r}}_i = \sum_{\substack{j=1 \\ j\neq i}}^{N} \frac{e^2}{4\pi\epsilon_0}\frac{\mathbf{r}_j - \mathbf{r}_i}{|\mathbf{r}_j - \mathbf{r}_i|^3} + e\mathbf{E}_E(\mathbf{r}_i), \tag{11}$$

with $\mathbf{E}_E$ as the externally applied acceleration field. In this approach all Coulomb effects are calculated from first principles. It therefore automatically covers the Boersch effect, trajectory displacement, and space-charge effects.[14]

For the external field we start from an analytical expression for the potential due to an infinite perfectly conducting plate at $z=0$ with a circular hole with radius a, which separates a uniform electric field $E_0\hat{z}$ at $z=-\infty$ from a zero electric field at $z=+\infty$,[20]

$$V_E(\mathbf{r}) = \frac{E_0 a}{\pi}\left[\sqrt{\frac{\rho-\mu}{2}} - \frac{|z|}{a}\arctan\sqrt{\frac{2}{\mu+\rho}}\right], \tag{12}$$

where $\mu = (x^2+y^2+z^2)/a^2 - 1$ and $\rho = \sqrt{\mu^2 + 4z^2/a^2}$. The origin of the coordinate system is at the center of the circular hole and the z axis is perpendicular to the conducting plate. If a voltage $V = E_0 d$ is applied across two such plates, separated by a distance $d \gg a$, then the electric field is given by $\mathbf{E}_E = \mathbf{E}_E^+ - \mathbf{E}_E^-$, where

$$\mathbf{E}_E^{\pm}(\mathbf{r}) = -\nabla V_E\left(x, y, \frac{d}{2} \pm z\right) + E_0\hat{z}H\left(z \pm \frac{d}{2}\right), \tag{13}$$

with H as the Heaviside step function. Equations (12) and (13) provide us with a convenient way to accurately describe the nonuniform acceleration field of a diode as shown in Fig. 1, which contains all the features of a real field, and which can be varied with only two parameters: The aperture radius a and spacing d.

All initial particle coordinates are chosen randomly in an uncorrelated way to correctly model the stochastic nature of the ionization process. The initial transverse position distribution is uniform within radius R. The initial longitudinal distribution is Gaussian with rms width σ_L. The initial velocity distribution is thermal with temperature T (and, hence, $\sigma_{v_x} = \sigma_{v_y} = \sigma_{v_z} = \sqrt{kT/m}$). The appearance of new particles in time is modeled by a Poisson process with rate I/e reflecting the random arrival times of the atoms in the ionization volume.

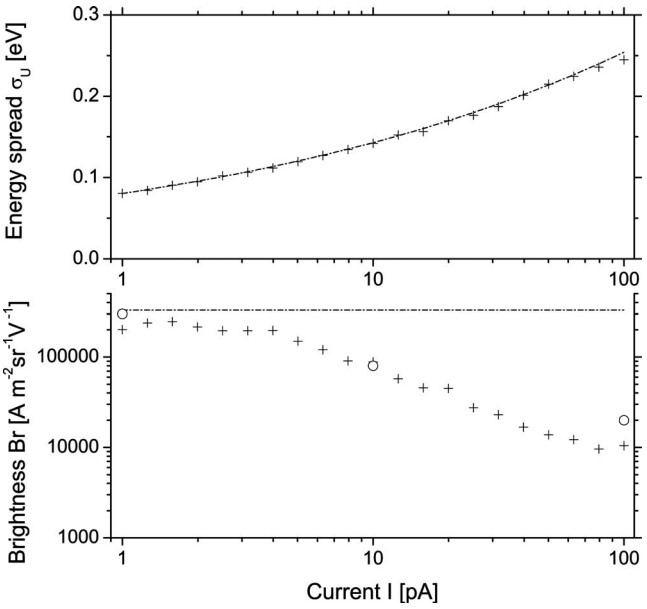

FIG. 2. Crosses: simulated rms energy spread (top) and reduced brightness (bottom) as function of current; open circles: reduced brightness calculated using transverse beam temperatures; and dash-dotted lines: fundamental limits calculated using Eq. (4) (bottom) and Eq. (10) (top).

V. RESULTS

The setup shown in Fig. 1 has been simulated with the GPT code for a large number of currents ranging from 1 to 100 pA. The starting point is a rubidium MOT with a temperature $T=200\ \mu$K, corresponding to velocities $v_{\text{th}}=0.22$ m/s, and a density $n=10^{18}/\text{m}^3$. A voltage $V=2$ kV is applied across a $d=20$ mm gap, resulting in an electrostatic field $E_0=100$ kV/m and an initial energy spread in the subelectron-volt range, see Eq. (10). The radius a of the aperture is 1 mm, which turns out to be sufficiently large to prevent that nonlinear fields affect the quality of the extracted beam. The particle distribution is analyzed 20 mm from the MOT center, i.e., 10 mm downstream from the aperture.

In Fig. 2 the resulting rms energy spread (top) and peak reduced brightness (bottom) are plotted as function of current. Figure 2 also shows the fundamental limits for the energy spread and brightness according to Eqs. (10) and (4). Figure 3 shows the transverse phase space distribution (top row), the energy distribution (middle row), and the uncorrelated angular distribution (bottom row) for beam currents $I=1$, 10, and 100 pA. In the following we will first treat the energy spread, followed by a discussion of the transverse phase-space distribution, disorder-induced heating, and the reduced brightness. We end with a prediction of attainable spot size in a FIB instrument.

A. Energy spread

The energy distributions shown in Fig. 3 clearly reflect the Gaussian intensity profile of the ionization laser beam. The solid lines are Gaussian fits from which the rms widths σ_U are determined. The centers of the Gaussian energy distributions are shifted by about 0.1 eV from the 1 keV final energy due the fact that the particles have not reached their final energy yet at the observation plane, see Eq. (12). In Fig. 2 the values of σ_U resulting from the simulations are plotted

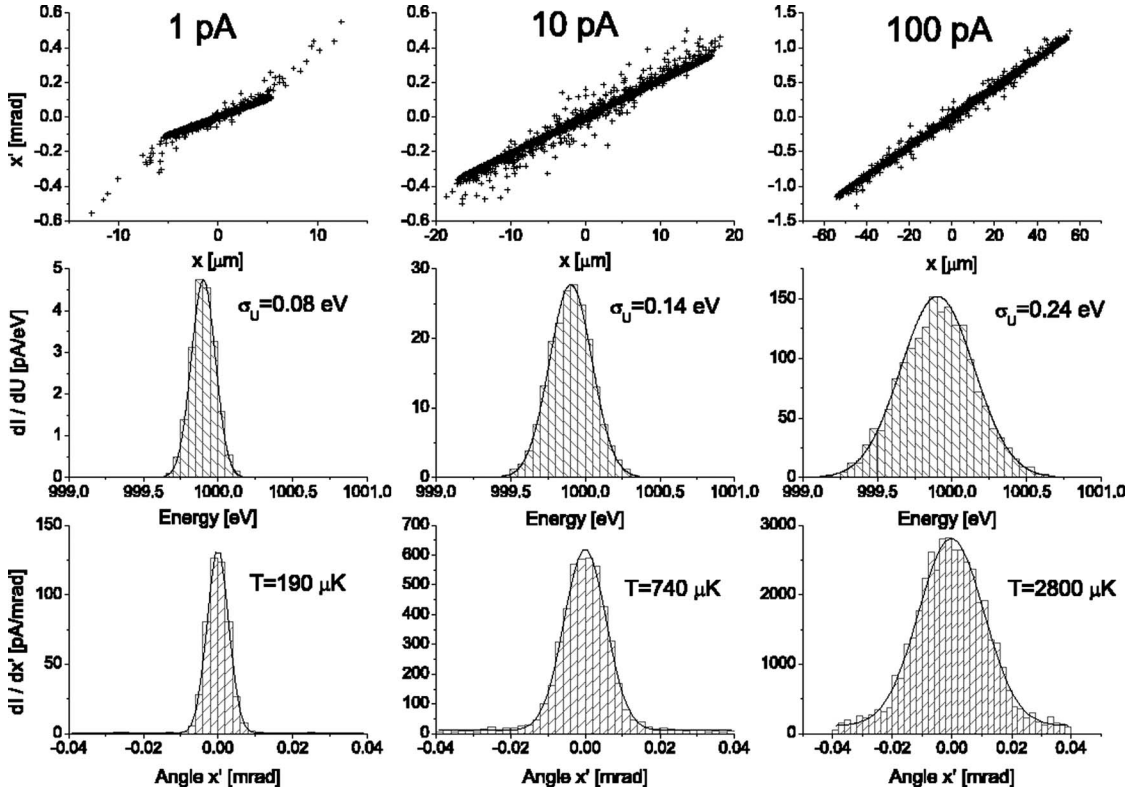

FIG. 3. Transverse phase space distribution (top row), energy distribution (middle row), and uncorrelated angular distribution (bottom row) for $I=1$, 10, and 100 pA. Note the changing scales. The solid lines are Gaussian fits.

as a function of current. Also plotted is the dependence of σ_U on current according to Eq. (10), indicated by a dash-dotted line, which gives a fundamental lower limit for the energy spread.

It is clear that the simple geometrical model for the energy spread, discussed in Sec. III, provides an accurate description: for small currents, which require a small initial beam radius R, the rms thickness σ_L of the ionizing sheet beam can also be chosen small, so the ions can be extracted from an increasingly narrow cross section. This leads to an increasingly lower energy spread that ranges from below 0.3 eV at high current (100 pA) to below 0.1 eV at low current (1 pA).

B. Phase-space distribution

The slant in the transverse position (x)-angle (x') phase-space distributions in Fig. 3 shows that diverging beams are created, which is mainly due to the negative lens effect or "exit kick" of the aperture. For a particle beam starting from zero velocity at the center of a diode with $a \ll d$ it can be shown that the focal length is given by $F=-2d$, i.e., $F=-40$ mm in our case. The negative lens gives rise to a linear correlation between transverse position x and angle x' with a slope $dx'/dx=F^{-1}=25\ \mathrm{m}^{-1}$. This is in good agreement with the results of the simulations for all three currents, implying that the effect of space charge on the beam divergence is small.

Apparently, the overall behavior of the ion beams is very similar for all three currents. A closer inspection, however, of the transverse phase space distributions in Fig. 3, reveals some subtle and interesting differences: the 1 pA beam has a well-defined narrow core and a halo consisting of particles which are scattered out of the core; for 10 pA the relative size of the halo is much smaller, while at 100 pA there are hardly any outliers. To further investigate the differences we show the uncorrelated angular distributions in the bottom row of Fig. 3. These distributions have been extracted from the top-row full phase space distributions by first removing the linear correlation, i.e., by collimating the beam with an ideal positive lens, thus minimizing the angular widths, and subsequently making histograms of the angular distributions of the particles. These angular distributions are fitted with a Gaussian profile, as is shown in Fig. 3. The Gaussian angular distribution corresponds to a thermal transverse velocity distribution, from which the transverse temperature T_t can be extracted. We find at $I=1$ pA a transverse beam temperature $T_t=190\ \mu\mathrm{K}$ which is virtually the same as the original ion temperature $T=200\ \mu\mathrm{K}$. At higher currents there is significant heating of the transverse degrees of freedom: $T_t=740\ \mu\mathrm{K}$ at $I=10$ pA and $T_t=2800\ \mu\mathrm{K}$ at $I=100$ pA.

C. Disorder-induced transverse beam heating

The rise of the transverse beam temperature, and the concomitant decrease in brightness, can be attributed to disorder-induced heating:[16] immediately after ionization the ions move with the very small velocities of the cold atomic gas, which means their kinetic energy is much smaller than the excess potential energy arising from their random spatial distribution. Subsequently the excess potential energy is converted into random motion of the ions and therefore into thermal energy.

Disorder-induced heating in a stationary ultracold plasma will lead to a final temperature T_f of the order of the Coulomb interaction energy between neighboring ions[16]

$$kT_f \approx \frac{e^2}{4\pi\epsilon_0 a}, \tag{14}$$

where $a=(4\pi n/3)^{-1/3}$ is the Wigner–Seitz radius and n the ion density. This final temperature is reached on a time scale of the order of the inverse plasma frequency $\omega_p^{-1}=\sqrt{m\epsilon_0/ne^2}$. In our system the initial ion density n_0 at the onset of the acceleration process is approximately given by

$$n_0 \approx \Phi\sqrt{\frac{m}{eE_0\sigma_L}} \approx 10^{14}\ \mathrm{m}^{-3}, \tag{15}$$

implying that a temperature $T_f \approx 1$ K is reached within $\omega_p^{-1} \approx 1\ \mu$s, which is approximately the time it takes for the ions to reach the observation plane. However, this final temperature is never reached, because the density decreases as the particles are accelerated, both lowering the final temperature and slowing down the heating process. Nevertheless, only a small amount of disorder-induced heating is sufficient to explain the observed temperature rise.

In principle disorder-induced heating only depends on the current density, and should therefore not increase with current. However, this only holds if the system size is much larger than the average interparticle spacing. In our case the average interparticle spacing at initiation is approximately $n_0^{-1/3} \approx 20\ \mu$m, which is larger than the transverse beam size $2R=9\ \mu$m at 1 pA, but smaller than the transverse beam size $2R=90\ \mu$m at 100 pA. Obviously, no disorder-induced transverse beam heating will occur if there are no neighbors in the transverse direction. In this so-called "pencil beam" regime the asymptotic behavior toward zero current, and thus to zero transverse size, is that there is no transverse heating and hence no reduction in brightness. On the opposite side of the current range, at 100 pA, we are nearing the "Holtsmark" regime. Here, the transverse size is so large compared to the interparticle spacing that heating becomes independent of current. Disorder-induced heating of the transverse degrees of freedom is therefore suppressed at $I=1$ pA, becomes increasingly important at higher currents, and starts to level off at 100 pA, in agreement with the simulation results shown in Fig. 2.

To check whether there are any other heating effects contributing, we did simulations in which the ions are started from an ordered "Hammersley" lattice[21] instead of a random distribution, but which are in all other aspects identical to the simulations presented in the earlier sections. In these simulations we find that no significant heating occurs, implying that other heating mechanisms are less important, at least in the first stages of acceleration. As a separate check we did simulations in which the initial energy spread was artificially decoupled from the extracted current. This did not affect the transverse heating at all, implying that the transverse temperature does not depend on energy spread. This shows that

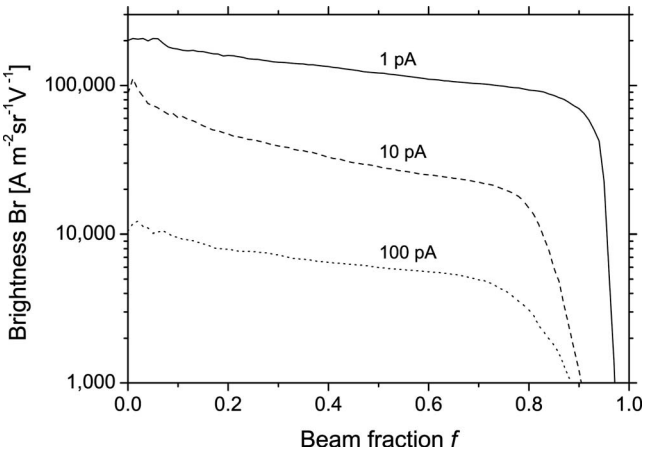

FIG. 4. Average brightness as function of beam fraction for 1, 10, and 100 pA.

there is no significant transverse heating due to equilibration between the relatively "hot" longitudinal degrees of freedom and the relatively "cold" transverse degrees of freedom: the transverse heating cannot be attributed to a reverse version of the Boersch effect.

D. Reduced brightness

By substituting the current density at the observation plane, $J=1.6\times10^{-2}$ A/cm^2, and the transverse temperature T_t obtained from the Gaussian fits in Fig. 3 into Eq. (2), we find for the reduced brightness at the observation plane $B_r=3\times10^5$ A m^{-2} sr^{-1} V^{-1} at $I=1$ pA, $B_r=8\times10^4$ A m^{-2} sr^{-1} V^{-1} at $I=10$ pA, and $B_r=2\times10^4$ A m^{-2} sr^{-1} V^{-1} at $I=100$ pA. These estimates are indicated by open circles in Fig. 2. The observed decrease of the reduced brightness with beam current is due to transverse beam heating and can therefore be attributed entirely to statistical Coulomb effects.

Equation (2) allows us to make an estimate of the reduced brightness, but it is not immediately clear whether the value of B_r thus obtained represents the entire beam (the average brightness), or only a very small part (peak brightness), or something in between. For this reason a robust calculation of the reduced brightness of the simulated beams has been done, based on the definition given in Eq. (1), using a numerical approach[22] outlined in the Appendix. This method allows us to unambiguously calculate the average reduced brightness of any fraction of the beam, including the peak brightness. Figure 2 shows the peak brightness calculated in this way (crosses), as a function of the total beam current.

The calculated curve agrees very well with the estimates based on Fig. 3. We find that at 1 pA the peak brightness is close to the fundamental limit of a few times 10^5 A m^{-2} sr^{-1} V^{-1}, indicated by a dash-dotted line. For higher currents the peak brightness gradually decreases due to statistical Coulomb effects to about 10^4 A m^{-2} sr^{-1} V^{-1} at 100 pA.

Figure 4 shows the average brightness as function of beam fraction, for $I=1$, 10, and 100 pA, obtained by numerically skimming off the beam by removing outliers according to the recipe in the Appendix. The overall behavior for all currents is identical: only a small fraction, on the order of 10%, needs to be skimmed to obtain very good average brightness. This is most pronounced for the 1 pA case, where reducing the current by 10% results in an average brightness which is larger than half the peak brightness.

E. Attainable FIB spot size

The high brightness and low energy spread of the UCI makes it an ideal source for a FIB instrument. In order to estimate attainable spot size as function of current we assume downstream electrostatic acceleration to a typical value of $V_p=30$ kV. The accompanying decrease in ion density allows us to assume that downstream heating effects are negligible compared to the heating already accounted for at the source. The spot size d_p is given by[14]

$$d_p=\left(\frac{IC_c^2\sigma_U^2}{B_rV_p^3}\right)^{1/4}, \tag{16}$$

where C_c is the chromatic aberration coefficient of the focusing system. If we assume a realistic $C_c=20$ mm, the expected spot sizes are 9.6 nm at 100 pA, 2.4 nm at 10 pA, and 0.8 nm at 1 pA.

VI. CONCLUSION

On the basis of particle tracking simulations of an ultracold ion source, using realistic acceleration fields and including all Coulomb interactions, we conclude that reduced brightness values in the order of a few times 10^5 A m^{-2} sr^{-1} V^{-1} are attainable at an rms energy spread below 0.1 eV. In comparison, the best quoted value for the LMI source is a reduced brightness of 10^6 A m^{-2} sr^{-1} V^{-1} at an energy spread of 4.5 eV.[1,6,7] The combination of high brightness and low energy spread of the ultracold ion source allows 100 pA to be focused on a 10 nm spot, whereas a subnanometer spot size is feasible if the current is reduced to 1 pA.

ACKNOWLEDGMENTS

This research is supported by the Dutch Technology Foundation STW, applied science division of the "Nederlandse Organisatie voor Wetenschappelijk Onderzoek (NWO)" and the Technology Program of the Ministry of Economic Affairs. This work is also part of the research program of the "Stichting voor Fundamenteel Onderzoek der Materie (FOM)," which is financially supported by NWO. We gratefully acknowledge Dr. P. Kruit for fruitful discussions and stimulating comments.

APPENDIX: BRIGHTNESS CALCULATION

Inspired by Ref. 22 the following procedure was used to calculate the reduced brightness for any fraction of the beam, and to obtain a robust estimate for the peak brightness. The input of the algorithm is the discrete set of transverse phase space particle coordinates $\mathbf{x}_i=(x_i,y_i,x_i',y_i')$, where $i=1,2,\cdots,N$ with N the total number of particles in the beam.

We start from the definition of the average brightness of the entire beam $\bar{B}_r$, which naturally follows from integrating Eq. (1) over transverse positions and angles

$$\bar{B}_r = \frac{I}{U\epsilon}, \tag{A1}$$

with ϵ as the four-dimensional (4D) hypervolume in (x,y,x',y') space, occupied by all the particles in the beam as they pass the observation plane. Because of the discrete nature of the particle distribution, the 4D volume ϵ can in principle be calculated in many ways.

We define ϵ as the volume of a 4D hyperellipsoid, whose shape and orientation are extracted from the 4×4 beam sigma matrix

$$\boldsymbol{\Sigma} = \begin{pmatrix} \langle xx\rangle & \langle xx'\rangle & \langle xy\rangle & \langle xy'\rangle \\ \langle x'x\rangle & \langle x'x'\rangle & \langle x'y\rangle & \langle x'y'\rangle \\ \langle yx\rangle & \langle yx'\rangle & \langle yy\rangle & \langle yy'\rangle \\ \langle y'x\rangle & \langle y'x'\rangle & \langle y'y\rangle & \langle y'y'\rangle \end{pmatrix}, \tag{A2}$$

where $\langle\cdots\rangle$ indicates averaging over the entire distribution. The directions of the principal axes of the ellipsoid are given by the eigenvectors of the sigma matrix and the lengths of the principal axes follow from the corresponding eigenvalues.

The hyperellipsoid as defined by Eq. (A2) can be scaled simultaneously in all four dimensions, such that both the orientation and aspect ratios remain constant. Once a point lies on the surface of such a scaled hyperellipsoid, it will remain on this surface for any downstream linear transport system. Although the shape and orientation of the ellipsoid will vary according to the beamline optics, its volume will remain constant. The volume ϵ_i of a scaled hyperellipsoid which just touches the 4D phase space position $\mathbf{x}_i$ is given by

$$\epsilon_i = \frac{\pi^2}{2}\sqrt{\det(\boldsymbol{\Sigma})}(\mathbf{x}_i^T\cdot\boldsymbol{\Sigma}^{-1}\cdot\mathbf{x}_i)^2. \tag{A3}$$

Using Eqs. (A2) and (A3) the set $\{\epsilon_i | i=1,2,\cdots,N\}$ can be generated. By sorting the list of ϵ_i values and renumbering them in such a way that $\epsilon_1<\epsilon_2<\cdots<\epsilon_N$, we may now define a unique curve of average brightness as function of beam fraction $f_i=i/N$,

$$\bar{B}_r(f_i) = \frac{1}{U}\frac{f_i I}{\epsilon_i}. \tag{A4}$$

Clearly, for calculation of the average brightness of the entire beam the volume $\epsilon=\epsilon_N$ should be used. The peak brightness $B_{r,\mathrm{peak}}$ is obtained by linear extrapolation of the $\bar{B}_r(f)$ curve to zero beam fraction $f=0$. This is a robust implementation of the definition given in Eq. (1), avoiding inaccuracies arising from the fact that when going to zero beam fraction, the number of data points, over which one should average, also goes to zero.

As a refinement to the procedure, already suggested in Ref. 22. we use the earlier method iteratively and base the sigma matrix from Eq. (A2) on the 50% particles with the smallest ϵ in order to prevent that outliers affect the overall shape of the ellipsoids.

[1] J. Orloff, M. Utlaut, and L. Swanson, *High Resolution Focused Ion Beams: FIB and Its Applications* (Kluwer Academic, New York, 2003); for a more compact overview see J. Orloff, Rev. Sci. Instrum. **64**, 1105 (1993).

[2] R. Rosenkranz, Application of FIB in Physical Failure Analysis, Infineon Technologies Dresden, Germany, review lecture at EFUG 2005, available from http://www.imec.be/efug/EFUG2005_Rosenkranz.pdf.

[3] M. J. Vasile, R. Nassar, J. Xie, and H. Guo, Micron **30**, 235 (1999).

[4] M. W. Phaneuf, Micron **30**, 277 (1999).

[5] For a recent measurement of most properties see R. Mühle, M. Döbeli, and C. Maden, J. Phys. D **32**, 161 (1999).

[6] J. C. Beckman, T. H. P. Chang, A. Wagner, and R. F. W. Pease, J. Vac. Sci. Technol. B **14**, 3911 (1996).

[7] G. D. Alton and P. M. Read, J. Appl. Phys **66**, 1018 (1989); Nucl. Instrum. Methods Phys. Res. B **54**, 7 (1991).

[8] L. Wang, J. Vac. Sci. Technol. B **15**, 833 (1997).

[9] J. Gierak, A. Septier, and C. Vieu, Nucl. Instrum. Methods Phys. Res. A **427**, 91 (1999).

[10] B. G. Freinkman, A. V. Eletskii, and S. I. Zaitsev, Microelectron. Eng. **7374**, 139 (2004).

[11] B. J. Claessens, S. B. van der Geer, G. Taban, E. J. D. Vredenbregt, and O. J. Luiten, Phys. Rev. Lett. **95**, 164801 (2005).

[12] J. L. Hanssen, J. J. McClelland, E. A. Dakin, and M. Jacka, Phys. Rev. A **74**, 063416 (2006).

[13] H. Metcalf and P. van der Straten, *Laser Cooling and Trapping* (Springer, New York, 1999).

[14] P. Kruit and H. Jansen, in *Handbook of Charged Particle Optics*, edited by J. Orloff (CRC Press, New York, 1997).

[15] P. W. Hawkes and E. Kasper, *Principles of Electron Optics, Vol. 2: Applied Geometrical Optics* (Academic, London, 1989), p. 976.

[16] Y. C. Chen, C. E. Simien, S. Laha, P. Gupta, Y. N. Martinez, P. G. Mickelson, S. B. Nagel, and T. C. Killian, Phys. Rev. Lett. **93**, 265003 (2004).

[17] See, e.g., T. C. Killian, S. Kulin, S. D. Bergeson, L. A. Orozco, C. Orzel, and S. L. Rolston, Phys. Rev. Lett. **83**, 4776 (1999).

[18] W. Ketterle, K. B. Davis, M. A. Joffe, A. Martin, and D. E. Pritchard, Phys. Rev. Lett. **70**, 2253 (1993).

[19] See the homepage of the General Particle Tracer (GPT) at http://www.pulsar.nl/gpt.

[20] J. D. Jackson, *Classical Electrodynamics* (Wiley, New York, 1999).

[21] H. Niederreiter, *Random Number Generation and Quasi-Monte Carlo Methods* (SIAM, Philadelphia, 1992).

[22] E. B. Holzer, Nucl. Instrum. Methods Phys. Res. A **532**, 270 (2004).